Journal of
Applied Remote Sensing

RemoteSensing.SPIEDigitalLibrary.org

System-on-module-based long-life electronics for remote sensing imaging with CubeSats in low-earth-orbits

Tom Neubert
Heinz Rongen
Denis Froehlich
Georg Schardt
Markus Dick
Tobias Nysten
Egon Zimmermann
Martin Kaufmann
Friedhelm Olschewski
Stefan van Waasen

SPIE.

Tom Neubert, Heinz Rongen, Denis Froehlich, Georg Schardt, Markus Dick, Tobias Nysten, Egon Zimmermann, Martin Kaufmann, Friedhelm Olschewski, Stefan van Waasen, "System-on-module-based long-life electronics for remote sensing imaging with CubeSats in low-earth-orbits," *J. Appl. Remote Sens.* **13**(3), 032507 (2019), doi: 10.1117/1.JRS.13.032507.

System-on-module-based long-life electronics for remote sensing imaging with CubeSats in low-earth-orbits

Tom Neubert,[a,*] Heinz Rongen,[a] Denis Froehlich,[a] Georg Schardt,[a] Markus Dick,[a] Tobias Nysten,[a] Egon Zimmermann,[a] Martin Kaufmann,[b] Friedhelm Olschewski,[c] and Stefan van Waasen[a,d]

[a]Central Institute of Engineering, Electronics and Analytics, Electronic Systems (ZEA-2), Forschungszentrum Jülich, Jülich, Germany

[b]Institute of Energy and Climate Research (IEK-7), Forschungszentrum Jülich, Jülich, Germany

[c]University of Wuppertal, Institute for Atmospheric and Environmental Research, Wuppertal, Germany

[d]University of Duisburg-Essen, Faculty of Engineering, Communication Systems (NTS), Duisburg, Germany

Abstract. CubeSats have become very popular science platforms in the past decades, leading to a continuously increasing number of developers in the academic field. For science missions, customized payload electronics have to be developed, depending on measurement tasks and requirements. Especially for the deployment of complex remote sensing payloads, state-of-the-art performance is needed to provide operational control and specific data processing, e.g., for image sensors. Highly integrated system-on-module (SoM) architectures offer low resource requirements regarding power and mass, but moderate to high processing power capabilities. However, a requirement to use a standard SoM in a satellite is to quantify its radiation tolerance. The radiation environment has been modeled, estimating the hazards at module level and reducing the risks to an acceptable level by applying appropriate mitigation techniques. This approach results in a sensor electronics design that combines hardware and software redundancies to assure system availability and reliability for long-life science missions in low earth orbits. Integrated in a miniaturized limb sounding instrument for atmospheric remote sensing imaging, the payload electronics will be deployed on a technology demonstration satellite for in-orbit verification. [DOI: 10.1117/1.JRS.13.032507]

Keywords: CubeSat; system-on-module; long-life; remote sensing; imaging.

Paper 190069SS received Jan. 29, 2019; accepted for publication Jun. 19, 2019; published online Jul. 11, 2019.

1 Introduction

CubeSats have become popular in past decades, leading to an increasing number of developers and projects.[1] CubeSats originally started as cutting-edge educational platforms and rapidly transformed into very effective technology demonstration tools. Recently, they have been increasingly used for scientific purposes.[2]

With development of the CubeSat standard for research and education[3] and collaborations between industry, government, and universities, subsystems became available on the market at low costs, e.g., command and control units, communication devices, attitude determination and control units, deorbit mechanisms, power distribution systems, and energy storage units. Often, commercial off-the-shelf (COTS) components are used without modification to develop various CubeSat subsystems.[4]

In addition to the subsystems, customized payload electronics have to be developed depending on measurement tasks and requirements for science missions. Especially for integrating

*Address all correspondence to Tom Neubert, E-mail: t.neubert@fz-juelich.de

1931-3195/2019/$28.00 © 2019 SPIE

complex remote sensing payloads, state-of-the-art performance is needed to provide the operational control and specific data processing for image sensors. Applications with high-resolution, high-speed imaging instruments, acquisition sequence control, and image processing (e.g., data compression) force strong real-time requirements on the payload design. Limited downlink capabilities require the online reduction of the system data rates. In 2007, highly integrated processing circuits with reconfigurable logic that are suitable for online processing tasks were introduced for traditional space instruments.[5–7] In 2015, COTS solutions became available for CubeSat instruments, which are continuously improved.[8,9]

Forschungszentrum Jülich and University of Wuppertal started the Development Initiative for Small Satellites Exploring Climate processes by Tomography (DISSECT). The goal of DISSECT is to develop small instruments to measure spectrally resolved radiation in the upper atmosphere at high spatial resolution. A first prototype version of a miniaturized instrument with a spatial heterodyne spectrometer (SHS) was tested on a sounding rocket by a student team.[10] Other activities with imaging systems,[11] Earth observation platforms,[12] and remote sensing instruments[13,14] have been built for in-orbit-demonstration-and-verification missions with short mission duration. Recently, scientific long-term measurements with remote sensing instruments have become increasingly important for the modeling of the climate system.[15] This leads to a great interest for cost-effective reliable payload electronics with short development time and maximum performance.

Scientific missions realized by universities were mostly without any detailed analysis during the development process and resulted in lower mission success.[16] Reasons for this are limited resources for permanent staff specializing in satellite disciplines. Students have very limited experience and limited amount of time available to perform a detailed analysis using specialized tools. Therefore, designs are simpler, less capable with higher risk but at lower cost. In contrast, professional companies perform many analyses for a significantly increased understanding of the satellite design, resulting in higher costs and development times.

A trade-off between professional design approach and basic design strategies, e.g., "buy-and-fly" is necessary to increase mission success of long-term measurements in the academic field. With the "Careful COTS" approach described by Sinclair and Dyer,[17] a promising design strategy has been published. In combination with radiation requirements and verification strategies, these measures comply with academic budget and schedule limitations. This approach is in contrast to the professional one, published as radiation hardened assurance.[18,19]

This paper describes a reliable sensor electronics design for a mission lifetime of 3 years in LEO. Our approach is based on component selective hardening extending the "Careful COTS" strategy by using state-of-the-art COTS components combined with targeted mitigation measures to fulfill scientific mission objectives. The reference design hosts a reconfigurable system-on-module (SoM) architecture to achieve high processing performance and reliability and simultaneously achieve significantly reduced development time, cost, and requirements on circuit design expertise.

The electronics design process is split into four methodological steps: (1) modeling of the radiation environment with respect to the mission constraints targeting an estimation of the resulting radiation exposure and the need for shielding, (2) analyzing the radiation sensitivity of components and characterizing the probability of failure in orbit, (3) estimating a sufficient number of redundancy and mitigation solutions, including software techniques and hardware protection circuits, and (4) verifying the design by qualification tests.

2 Materials and Methods

2.1 *System-on-Module for Science Instrumentation*

To reduce development time and circuit design expertise and costs, an SoM architecture is used. This module is a board-level circuit that combines reconfigurable hardware as programmable logic with a processing unit, memory, and peripheral interfaces in a single module. It represents a high level design by including special functions (e.g., data processing, data compression, and interface control).

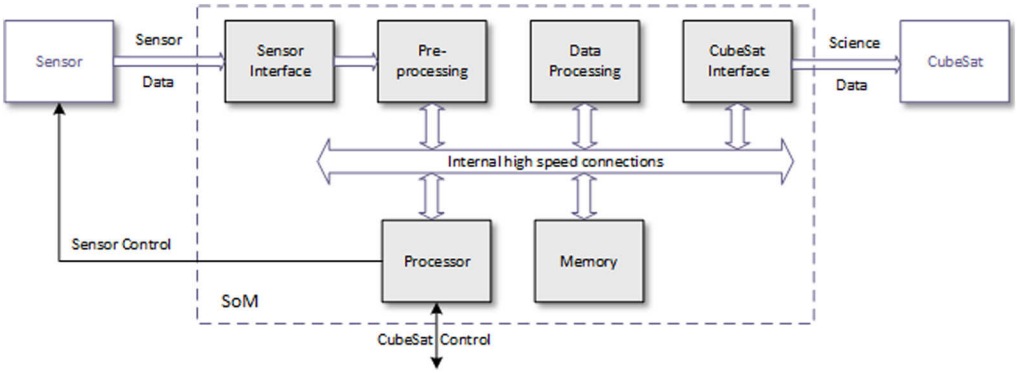

Fig. 1 Overview of functions inside an SoM architecture.

Figure 1 shows the general architecture of such an SoM and its functionality. Such highly integrated architectures have low resource requirements for power and mass, but high processing power capabilities. The major characteristics are flexibility, (re)programmability, modularity, and module reuse. Reuse is important as the deployment and implementation of complex systems becomes possible and affordable only when basic elements are present.[5] A further advantage of this architecture is that only a few additional components are needed to realize a scientific instrument's electronics. Additional components are a single power supply, individual converters for analog and digital signals that deal with the signals of the imaging sensors or detectors and a communication transceiver circuit to transmit data to the spacecraft.

SoMs are available in a variety of reconfigurable hardware architectures using field programmable gate arrays (FPGA) as a kind of (S)RAM-based devices also with directly integrated ARM or PowerPC processors or as single microcontrollers. These modules will typically provide several interfaces (e.g., RS232, I2C, SPI, CAN, etc.) to accommodate a wide range of users and to ease the task of interfacing with peripheral devices and other controllers.

In this paper, we used the state-of-the-art COTS SoM TE0720-03-2IF, which is based on a Xilinx Zynq 7020 system-on-chip (SoC) with configuration flash and nonvolatile DDR-3 memory. More details about the hardware used can be found in Sec. 3.2.

2.2 *Radiation Environment Modeling*

The hazards to the electronics are driven by orbit trajectories. Typical LEOs are referred to as Sun Synchronous, Polar and Equatorial orbits. The space radiation environment consists of high energy solar particles and photons, charged particles trapped in Earth's magnetic field, and galactic cosmic rays (GCRs). The largest sources of ionizing radiation in LEO are trapped proton and electrons, while particles with solar origin dominate for higher orbits and interplanetary missions. The total ionizing dose (TID) is accumulated over the entire mission life, which can lead to wear out or aging, causing threshold shifts and leakage that increases over time and orbit. Nominal single event effect (SEE) rates would be driven by GCR as a background, with proton contributions from trapped particles as well as solar wind.

The first step in the design approach is to calculate the radiation environment with respect to the mission constraints, resulting in an estimation of the TID and the need for shielding. There are a number of models that can be used to predict radiation environment for a mission. Several of these models are integrated into the online tool SPENVIS,[20] which allows the user to define the spacecraft orbit, and to compute unshielded and shielded particle fluxes and radiation doses.

In this study, SHIELDOSE-2 in SPENVIS is used to calculate the ionizing dose at the center of a solid aluminum sphere, as a function of sphere radius where irradiation is applied from all directions. The trapped electrons are significantly reduced by increasing the thickness of shielding, while the trapped protons are reduced only slightly. A typical dose depth curve is shown in Fig. 2 for the accumulated radiation dose (in rad) depending on the shielding thickness for a 3-year mission lifetime.

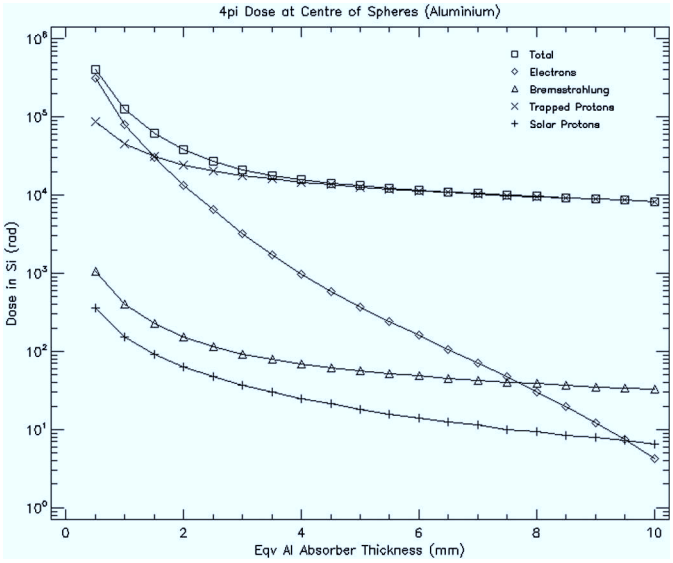

Fig. 2 Effective dose versus aluminum shielding thickness for a 3-year LEO mission ($h = 1100$ km).

The calculation indicates that below 1.5 mm of shielding, trapped electrons are the dominant radiation source, where above 1.5 mm of shielding, trapped protons dominate. Apart from this, it is noticeable that the total ionizing cannot be reduced further for aluminum absorber thicknesses larger than 6 mm due to trapped protons, which cannot be shielded effectively. The effective shielding has to be determined by using sectoring analysis.[21] The method assumes that all of the radiation sensitive electronics are combined in a single point in the center of a sphere. Next, absorption relevant obstacles in similar directions, interposed between the electronics and the instrument boundaries, are grouped into elements (e.g., chassis side, front optics, etc.). For each element, the absorption properties are translated into an equivalent absorber thickness for aluminum. Finally, the fraction of a sphere surface (%) is calculated for each element and referred to as shielding sector. The effective ionizing dose value at the electronics can be calculated by summing up the ionizing dose values for each shielding sector.

To reduce the weight of the shielding, graded-Z material constructions are used.[22] Graded-Z shielding is a laminate of several materials with different Z values (atomic numbers) designed to protect against ionizing radiation. Analysis conducted by Fan et al.[22] effectively demonstrated that a low-high-low-Z layering provides a 60% mass savings to achieve the same radiation attenuation levels as a single layer of aluminum. However, while graded-Z shielding can be more mass efficient than a single layer of aluminum, it normally requires more volume, which can be a critical design issue in highly integrated CubeSat systems.

2.3 *Analyzing the Component Radiation Sensitivity*

In a second step, the effective SEE sensitivity of the electronic components on orbit is determined by analyzing and characterizing their radiation sensitivity. SPENVIS is used to calculate the orbit averaged proton flux that shows the proton energy spectrum behind the shielding.

Related upset rates on orbit can be approximated with single event upset (SEU) rates found by tests at proton or heavy ion test facilities for components under consideration. Using available radiation test data, rather than conducting a radiation lot acceptance testing campaign, can reduce costs. For estimation of the radiation effect on component level, space agencies provide databases.[19,23] However, part or lot variations generally are to be captured. Part-to-part and lot-to-lot variation can be attributed to the manufacturing process. If a manufacturer changes foundries or changes the process to increase performance, large changes in the radiation response can be seen.[24] SEE testing or data can benefit from the knowledge that a mask set and process have not changed, whereas TID results are much more process oriented with dependencies on

how oxides and interfaces are manufactured and can vary on small deviations in the temperature, doping, or chemical process steps. Lot-to-lot variations can be covered sufficiently by using a radiation design margin (RDM). The RDM is defined as the ratio of the part or component radiation capability in the given application to the expected radiation environment at the part or component location during the mission. Based on flight experiences, it is common practice for most applications to require an RDM of 2 or more for COTS parts with limited test data. The guidelines and recommendations of the minimum data necessary to quantify a risk to the system can be considered as shown by Campola et al.[25]

SEU response data sets can be fitted with a Weibull curve function to facilitate orbital rate calculations[26]

$$\sigma(\mathrm{LET}) = \sigma_0 \cdot \left[1 - e^{-\left(\frac{\mathrm{LET}-\mathrm{LET}_{th}}{W}\right)^s}\right], \tag{1}$$

where σ_0 is the limiting or plateau cross section, LET_{th} is the linear energy transfer (LET) threshold parameter, W is the width parameter, and s is the dimensionless exponent. Figure 3 shows a cross section ($\mathrm{cm}^2/\mathrm{bit}$) versus LET value ($\mathrm{MeV} \cdot \mathrm{cm}^2/\mathrm{mg}$) for a device in our design as input parameter for SPENVIS.

The total number of SEUs for the whole mission is computed considering the proton orbit flux, using cross section characteristics and the rectangular parallelepiped (RPP) method,[27] which characterizes the sensitive volume of the device. The RPP values are given by the device test reports or can be approximated with $x^2 \approx y^2 \approx \sigma_0$, $z = 2$ μm and are needed as additional input parameters for the simulation.[28] With SPENVIS, the effective proton flux will be estimated using the AE9/AP9 model.[29,30] Considering the effectively used aluminum shielding thickness, an SEU rate will be calculated for every component.

Many passes through the Van Allen radiation belts or the South Atlantic Anomaly (SAA) lead to high doses or temporal SEE threats. Therefore, an analysis of its impact is needed to estimate further mitigation solutions due to significantly increasing values at upper LEO altitudes. Figure 4 shows the geographic location of the SAA above a defined integral flux margin for protons and electrons. SPENVIS is used in an additional analyze step to estimate the mitigated SEU rate, if SAA region will be excluded using a modified dataset for proton and electron fluxes.

The resulting upset rates are given in SEU events per bit. Additional values can be defined, as SEU per device or SEU per day where upset rates per component or lifetime are normalized. Especially for memory and programmable logic components, the degree of use in the final design needs to be considered for a more realistic characterization, see Table 3 in Sec. 3.2.

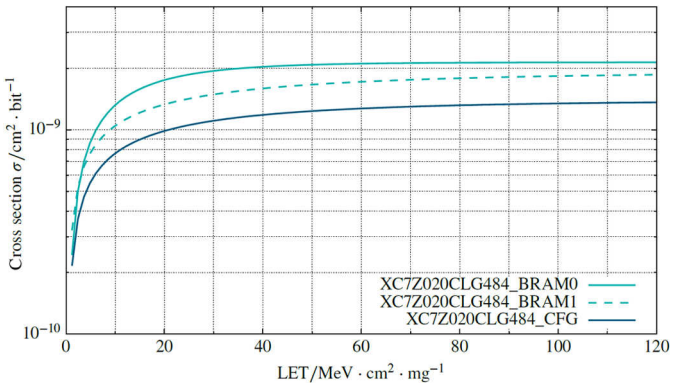

Fig. 3 Device component sensitivity given by cross sections for direct ionization for Xilinx Zynq XC7Z020 SoC.[26]

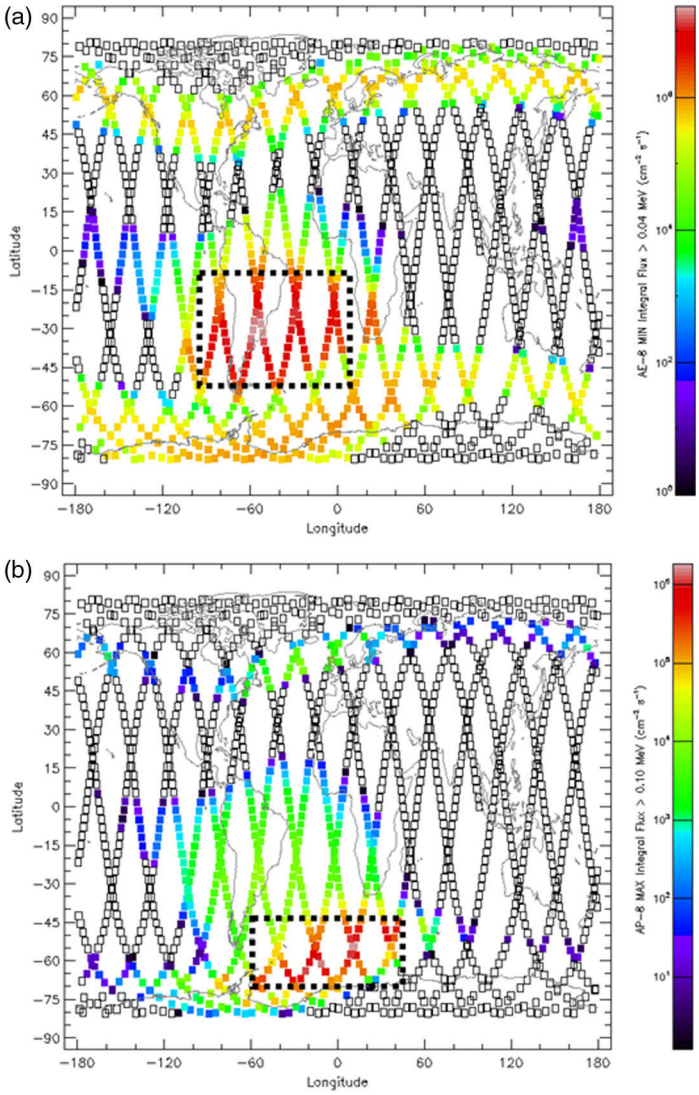

Fig. 4 Integral flux of (a) trapped electrons and (b) trapped protons in the Van Allen belt and localization of the SAA on the world map at 1100 km altitude.

2.4 *Mitigation Techniques and Protection Circuits*

By identifying the hazards and a representative model to which the parts are exposed, the electronics can be designed in a next step with mitigation techniques and protection circuits. Key factors that need to be considered are the criticality and usability of the COTS components in its application with respect to nondestructive and destructive SEEs.[31–33] For nondestructive SEEs (soft errors), the functionality of the circuit can be recovered. This includes single event transient (SET), SEU with multicell upset and multibit upset and single event functional interrupt (SEFI). Destructive SEEs describe hard errors that permanently damage the component parts and result in it being inoperable. Reasons are single event latch-ups (SEL), single-event gate ruptures (SEGR), and single-event burnouts (SEB).

2.4.1 *Mitigation techniques*

Mitigation techniques are needed to recover from faults and thereby increase the reliability. In particular, these techniques include circuit redundancy, functional redundancy, standby redundancy, and triple modular redundancy (TMR). A common fault-tolerance technique applied in electronics is to use circuit redundancy. Simple components such as resistors, capacitors, diodes,

and relays are connected in series and simultaneously in parallel. More complex components can use parallel redundancy if they can override each other; for instance, the input power supply circuit or communication transceiver components. Another useful technique is functional redundancy, wherein a required element of the system is not replicated but a similar function exists that can support degraded performance. For examples, if a nonvolatile memory unit fails, the electronics can continue as long as the power is maintained on the volatile storage. These techniques provide cost-effective backups when replication of the primary function is impractical. Long-life systems often rely on cold standby redundancy. In this concept, the spare components are turned off until needed to replace faulty units. The basic idea behind is that unpowered devices are less sensitive to radiation and have a longer lifetime than powered components. In TMR, a programmable logic is replicated three times and the output of the logic is determined by a majority vote.

TMR is an essential SEU mitigation technique for all long-life missions. For the estimation of the need of TMR granularity, a system error rate analysis has to be established. The SEU error rate R can be determined[34] with

$$\mathrm{R} = \frac{1}{T_C} - \frac{1}{T_C}\prod_{i=1}^{M}[3 \cdot e^{(-2 \cdot N_i \cdot r \cdot T_C)} - 2 \cdot e^{(-3 \cdot N_i \cdot r \cdot T_C)}], \tag{2}$$

where N_i represents the number of configuration bits in a single triplicated domain, T_C is the scrub time in seconds given by the designer, M is the number of groups also called TMR granularity, and r is the SEU rate per bit described in Sec. 2.3. For a small number of SEUs, the error rate can be approximated by

$$R \approx 3MT_C(\mathcal{M}_2 r)^2 (\text{small } r) \text{ and } \mathcal{M}_2 \equiv \left[\frac{1}{M}\sum_{i=1}^{M} N_i^2\right]^{1/2}, \tag{3}$$

where M_2 represents the weighted number of bits for every triplicated logic block. The number of groups M is estimated using a tool such as "FPGA editor" that can count the number of triplicated logic blocks (instantiations) given by name. Figure 5 shows error bit rates for different numbers of granularity M, where $M = 0$ shows the error rate without TMR implementation. In case of a partially mitigated design, where some logic blocks are not triplicate an adapted approximation is given by Allen et al.[35] with

$$R \approx M_U r + 3MT_C(\mathcal{M}_2 r)^3 \,(\text{small } r), \tag{4}$$

where M_U is the number of unmitigated configuration bits and r is the SEU rate per bit.

To mitigate errors in COTS SoMs, a combination of TMR with configuration memory scrubbing will be used. Configuration memory scrubbing periodically scans the entire device and

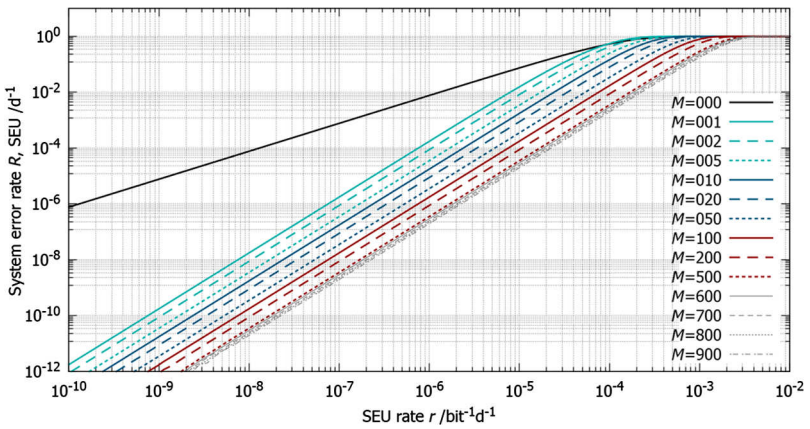

Fig. 5 System error rate R as a set of functions for different numbers of triplicated logic blocks M and a scrub time $T_C = 1$ d for a fully mitigated design.

corrects configuration memory errors by rewriting the memory frames containing them. Scrubbing can be implemented by simply overwriting all of the configuration frames, or by reading and comparing these frames with a reference image to replace any frame that is corrupted.

Redundancy solutions are sometimes not feasible, high reliable components are necessary to achieve long-life mission success. These have to be selected as radiation hardened components. Using prototype grades, form, fit, and functionally are identical to flight-grade components with the same die at much lower costs. Cost-intensive screenings were skipped, and these components are often classified as radiation tolerant.

2.4.2 *Protection circuits*

Hardware and software overcurrent protection circuits can be implemented to reduce SEL. A latch-up can lead to device failures, as all CMOS devices are susceptible to ionizing radiation particle strikes. When a device latches up, a paratactic structure on the CMOS die becomes forward biased and creates a short circuit from positive to negative power rails. Protection circuits can watch for elevated current levels and trigger a power reset to the offending circuit.

A watchdog timer (WDT) is a hardware circuit that is often used to monitor the state of a processor, to reset the processor, to scrub reconfigurable hardware when an SEU is detected, or to trigger a power cycle after a latch-up.

Error-correcting code (ECC) memory is capable of detecting and correcting bit errors in RAM and FLASH memory using checksums.[31] It is a very common mitigation technique and mostly available in COTS memory components.

3 Sensor Electronics Implementation

The electronics design presented in this work is designed for a CubeSat-sized remote sensing instrument for atmospheric research. The purpose of the Atmospheric Spatial Heterodyne Interferometer Next Exploration (AtmoSHINE) instrument is to measure temperatures in the mesosphere and lower thermosphere region. It contains an SHS to measure the rotational structure of the O_2 A-band from the Earth limb.[36] Figure 6 shows a three-dimensional CAD drawing of the instrument. Limb radiance enters from the left side. The electronics is accommodated in a box at the top-side of the instrument. The instrument is designed to fly in a Sun-synchronous near Earth orbit at an altitude of 1100 km during solar minimum conditions. Designed mission lifetime is 1 year.

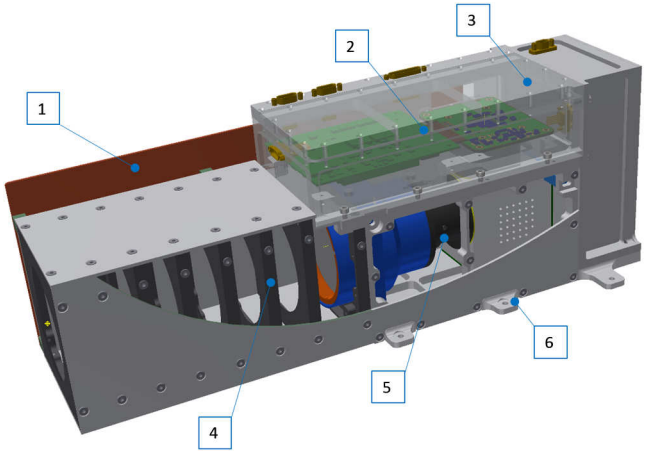

Fig. 6 Illustration of miniaturized limb sounder instrument with localization of potential shielding elements: (1) radiator plate, (2) sensor electronics, (3) chassis, (4) baffle, (5) front optics and SHS housing, and (6) base plate.

Table 1 Effective shielding thickness and total dose rates inside electronics.

Sphere surface (%)	Element	Equivalent aluminum thickness (mm)	Without satellite shielding		2 mm satellite shielding	
			3-year contributed dose (krad)	5-year contributed dose (krad)	3-year contributed dose (krad)	5-year contributed dose (krad)
35	Chassis side	2.5	9.5	16.1	5.0	7.8
16	Front optics and SHS housing	4.5	2.3	4.2	2.3	2.8
25	Radiator plate (copper)	8	2.4	4.0	2.0	3.2
8	Baffle	8	0.7	1.3	0.7	1.1
16	Base plate	10	1.3	2.2	1.3	2.0
TID			**16.2**	**27.8**	**11.3**	**16.9**

3.1 *Radiation Dose Rates inside Electronics*

The radiation dose rates were calculated for a mission lifetime between 3 and 5 years using SPENVIS. Therefore, the worst case scenario is used as design constraints together with a modified confidence level for a solar proton model given by Sinclair and Dyer.[17]

The radiation dose is calculated for various wall strengths for the electronics box. Satellite shielding is also considered, because the instrument will be accommodated inside the satellite structure.

In addition, the effective shielding has to be determined by some approximations using sectoring analysis. In Table 1, for each element, the contributed dose is derived from the results of the total dose simulation for the equivalent aluminum thickness (Fig. 2) by multiplying it with the corresponding fraction of the sphere surface. The effective TID inside the electronics is calculated by summing up the contributing dose values.

Based on the calculated results, the specification for the radiation tolerance of the electronic components can be specified. With a radiation tolerance of 20 krad, the electronics are functional for at least 3 years. By adding 2 mm of aluminum shielding to the satellite housing, it will operate for 5 years. Otherwise, an additional spot shielding must be attached to sensitive parts. These estimates provide the upper limits required for the radiation test.

3.2 *Component Selection and Radiation Sensibility*

The proper selection of a COTS SoM and additionally required semiconductor components is most important. Criteria for this are the functionality, performance, availability, alternate grade parts (AEC-qualified), and available data on irradiation tests. Regarding these criteria, the COTS module TE0720-03-2IF was selected as SoM component. This module is automotive grade and available in various designs with different hardware architectures. Individually adapted electronics can be developed with the same interfaces. In cooperation with the vendor, the on-module DDR3 memory was replaced by the compatible version with integrated ECC (IME1G16D3EEB). In addition to the memory ICs, the XA7Z020 Zynq System-on-Chip (SoC) from Xilinx covers all the functional requirements for the sensor electronics. With the flash memory 25FL256S, the configuration into the SoC is loaded during initialization. Radiation test data[26,37,38] and RPP parameter for component sensitivity analysis is given in Table 2.

With these module parameters, SEU rates are estimated using SPENVIS for the specific mission duration and the results are listed in Table 3. The results indicate an SEU rate for the flash memory of less than three events during mission (0.56/year) in contrast to the logical configuration memory (CFG), which will occur around three events per month.

Table 2 Cross section data as Weibull fit parameter and RPP parameter of SoM components.

Device	Data reference	σ_0 ($cm^2 \cdot bit^{-1}$)	LET_{th} ($MeV \cdot cm^2 \cdot mg^{-1}$)	W ($MeV \cdot cm^2 \cdot mg^{-1}$)	s	$x \cdot y$ (μm^2)	z (μm)
XA7Z020-CFG	Ref. 26	1.40×10^{-9}	0.5	14	0.6	3.70	2.0
XA7Z020-BRAM0	Ref. 26	2.14×10^{-9}	0.5	10	0.8	5.28	2.0
XA7Z020-BRAM1	Ref. 26	1.94×10^{-9}	0.5	15	0.56	3.94	2.0
NOR Flash	Ref. 37	1.41×10^{-10}	3.6	23.7	2.2	108.2	2.0
DDR3 RAM	Ref. 38	3.38×10^{-11}	0.47	57.6	3.6	64×10^3	2.0

Table 3 Error rate generated by SEUs during 5-year mission duration for SoM components.

Device	Degree of utilization	SEU rate per bit	SEU rate per device	Total errors (util.)	SEUs per day	SEUs per month	SEUs per year	SAA impact factor
XA7Z020-CFG	0.17	1.56×10^{-4}	1.10×10^3	190	0.104	3.160	37.9	0.23
XA7Z020-BRAM0	0.01	2.70×10^{-4}	6.97×10^2	10	0.005	0.166	2.0	0.24
XA7Z020-BRAM1	0.01	3.20×10^{-4}	8.26×10^2	12	0.006	0.197	2.4	0.23
NOR Flash	0.14	7.50×10^{-8}	2.01×10^1	3	0.002	0.047	0.56	N/A
DDR3 RAM	0.03	3.00×10^{-7}	3.22×10^2	10	0.006	0.168	2.0	0.24

These results imply that additional mitigation techniques are necessary to reduce the SoC error rate for the CFG and the logical block memory (BRAM). Considering SAA influences, a simple solution is to switch off the sensor electronics while passing this region. The SAA impact factor shown in Table 3 is calculated by excluding geographical regions with an integral flux rate of 1.5×10^5 $cm^{-2} \cdot s^{-1}$ for protons and 1.5×10^6 $cm^{-2} \cdot s^{-1}$ for electrons, see Fig. 4 in Sec. 2.3. Thus, the error rate, e.g., for BRAM1 is reduced by a factor of 4 and reaches only three SEU events during a mission period of 5 years. Certain components, e.g., passive ones (resistor, capacitors, inductors, etc.), single junction diodes and bipolar junction transistors as well as nonelectronic materials (PCB substrates) can be assumed to be radiation tolerant to at least 30 krad when operated in proper conditions.

3.3 *Hardware Design*

The sensor electronics design consists of two functional blocks, the proximity electronics (PXE) for directly interfacing to several detector ICs and the frontend electronics (FEE) with a SoM, which serves as the central processing system.

The FEE handles signals from the CubeSat bus to start the measurement, to acquire detector data, to provide data preprocessing (e.g., data binning), and to transfer data to the command and data handling (C&DH) subsystem. Figure 7 shows the block diagram of the AtmoSHINE sensor electronics. The PXE board is designed as universal sensor interface. For this application, a scientific CMOS detector, the HWK1910 with 1920×1160 pixel array, is attached to the PXE board. The HWK1910 is read out using a digital low voltage interface as data bus and configured using serial interfaces to set the field of view, the integration time, and the frame rate of selectable measurement scenes, see Fig. 8.

The internal power management is controlled by a build-in-self-test (BIST) sequence, which checks all power rails, the attached interfaces, and the subsystems. The result of the BIST is reported in a status register, which is included in the housekeeping data package. Furthermore,

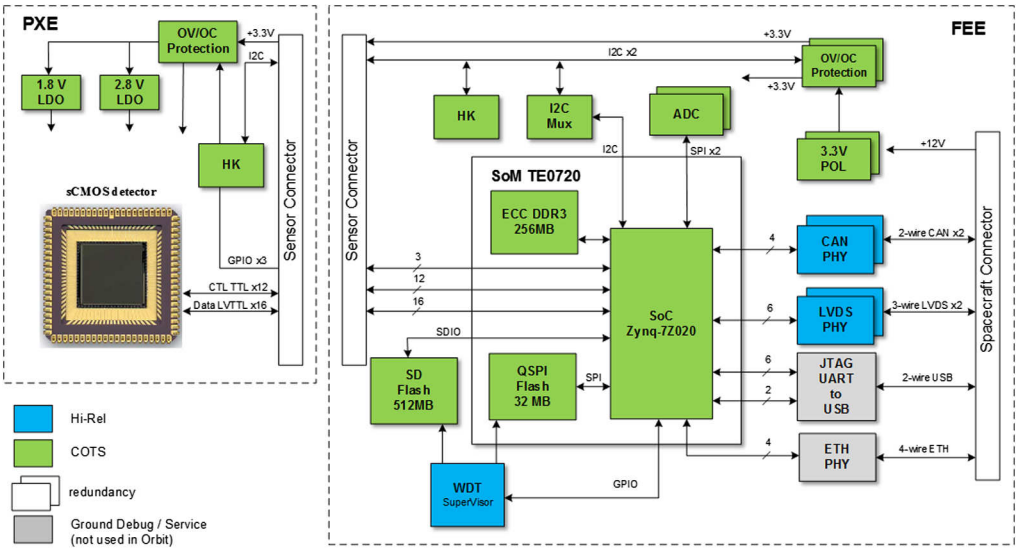

Fig. 7 Block diagram of AtmoSHINE sensor electronics with PXE for directly interfacing to several detector ICs and the FEE with a system on module as embedded controller.

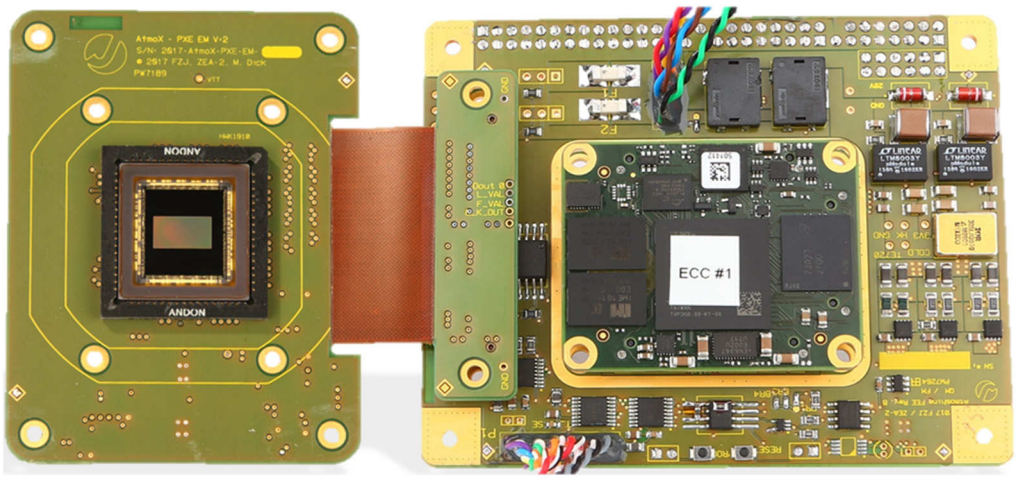

Fig. 8 AtmoSHINE sensor electronics with HWK1910 scientific CMOS detector at PXE and Xilinx Zynq 7020-based SoM (Trenz-TE0720) assembled at FEE.

the detectors, PXE and FEE, are protected against SEL using overcurrent protection circuits and the electronics can operate from common CubeSat bus voltages and use redundant point-of-load converters to generate the internal supplies.

The SoC operates as system controller and is protected by additional components around the SoM. It boots from an on-module QSPI flash memory or an industrial grade SD card providing a reference boot image in redundancy. The Delkin SE02SAMHL SD memory card is radiation tolerant up to a TID of 24 krad[39] and powered off during operation to avoid hazards with its biased control/interface circuit due to SEL. The radiation hardened WDT ISL706, which triggers a reset signal of the processor in case of a firmware violation, checks the operation of the system controller. The reset signal triggers a reconfiguration procedure due to powering up the SD card, and the reference boot image will be loaded into the logical fabric. The on-module volatile DDR-3 processor memory is protected by using memory chips with integrated ECC, periodic memory pattern, and cycling redundancy checks (CRC) on selected data-structures.

The communication is split up into two channels: A telecommand interface to control the instrument and acquire housekeeping values and a science data interface to send the detector data

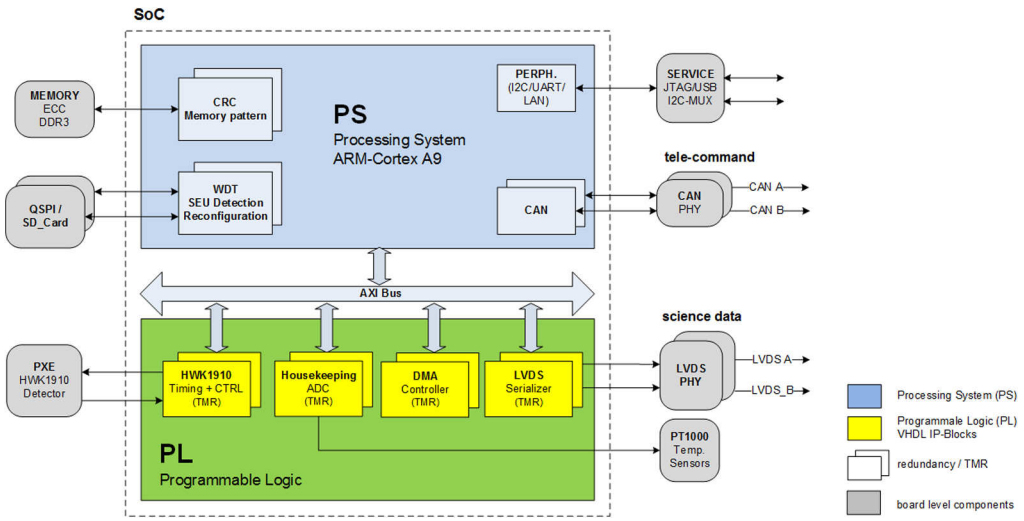

Fig. 9 Block diagram with SoC hardware and software structures and interconnections.

to the C&DH. Every channel is implemented as a redundant logic core and can be a combination of different physical interfaces in case of limited resources. The CAN interface uses the Hi-Rel ISL72027 transceiver to connect the control interface to the main payload and is duplicated into the processor. With a proprietary data interface including clock, data, and a trigger signal, science data are transmitted via a radiation tolerant SNJ55LVDS31 device with data rates up to 20 Mbps, which is protected with TMR inside the programmable logic.

Further parts of programmable logic configuration are placed in TMR, and the majority voters generate an index signal in the event of a discrepancy, which also triggers the WDT. TMR protected parts are: the detector timing and control interface, the housekeeping ADC elements, the LVDS science data interface, and DMA control unit, see Fig. 9. In this partially mitigated design, no mitigation is implemented for the AXI bus interface. Each subpart is triplicated with a granularity $M = 1$. This results in a resource utilization of 39.4% (slices), where the number of unprotected configuration bits is 12,800. The total number of TMR blocks M is estimated to be 27 and the number of bits per block Ni is determined using Xilinx PlanAhead tool. In case of an unmitigated implementation, the calculated error rate is three times per month (see Table 3) and will be reduced with this partially TMR design to 0.033 events or approximately once every 2.5 years using Eq. (4) in Sec. 2.4.1.

In case of functional operation errors, an in-orbit reprogramming mode is implemented. It uses the QSPI flash for acquiring the new image code. If the satellite receives a new program code update in orbit, both the original and the new code images are stored such that the system can recover to a known good state in the event of a problem during reprogramming. The reference boot image on the SD card will be overwritten only if the new image is verified successfully by CRC checks. Table 4 summarizes the implementation measures.

Additional interfaces are implemented for ground operations, testing, and qualification: an Ethernet interface to stream images for real-time calibration procedures, a USB interface as service terminal, and an in-system programming interface for firmware updates. These components are independently powered by the ground support equipment and switched off during mission.

4 Qualification Tests

Qualification testing ensures that the design is acceptable and that the electronics and the satellite will function in the expected environments and lifetime. These tests include (1) electromagnetic interference/compatibility (EMI/EMC) test, (2) burn-in functional stress test, (3) environmental tests (thermal vacuum), and (4) radiation tests. The satellite provider will perform mechanical qualifications with shock, random, and sinusoidal vibration tests during acceptance procedures.

Table 4 Overview sensor electronics mitigation.

Class	Type of measures	Mitigation effect	Devices/functionality
Component selection	Part classification	Degradation	Automotive COTS (AEC-Q 100)
	Hi-Rel	TID, SEE	Radiation tolerant @ single strain
Redundancy	Standby "cold"	SEE	SD-card with reference boot image
	Circuit "warm"	SEE	Power conversion
	Functional	SEU	BIST
	TMR	SEU	FPGA configuration logic
Protection circuits	WDT	SEE	Supervisor/reset/reconfiguration
	Over current/voltage	SEL, SET	SEL protection
	Power control	SEE, SEL	Power off during SAA passes
Memory protection	ECC	SEU	Volatile DDR-3 single bit protection
	CRC	SEU	In-orbit reprogramming verification
	Memory pattern	SEE	DDR-3 SDRAM
	Scrubbing/reconfiguration	SEU	FPGA configuration
Communication protection	Component selection	TID, SEE	Hi-Rel CAN and LVDS transceiver
	CRC	SEU	Command control verification

Table 5 MIL-STD461F requirements for the sensor electronics.

Test method	Test description	Frequency range
CE 102	Conducted emissions, electric field, space systems, and fixed wing external (limits)	10 kHz to 10 MHz
RE 102	Radiated emissions, electric field, space systems, and fixed wing external (limits)	150 kHz to 3 GHz

4.1 *Electromagnetic Interference and Compatibility Test*

The objective of the EMI/EMC test is to verify that the hardware will operate properly if subjected to EMI from other sources and that it does not generate EMI itself that might disturb operations of other systems. This test ensures that, under normal operating conditions, the subsystem does not have electromagnetic characteristics resulting in emissive, radiative, or conductive interference. The testing was performed to comply with the MIL-STD-461F standard that deals with conducted and radiated effects and is categorized into emissions and susceptibility. The EMI test requirements for the compliance of the electronics are listed in Table 5.

Our electronics passed the CE102 (conducted emissions) test with at least 20 dB μA and the RE102 (radiated emissions) test with 10 dB μV/m below the limit according to MIL-STD–461F.

4.2 *Burn-In Functional Stress Test*

To reduce the amount of rework and further qualification tests, a burn-in functional stress test is performed first. Depending on the test results, additional design tasks and further testing might

Table 6 Burn in functional stress test conditions for different temperatures.

Temperature in °C	45	50	55	60	65	70	75
Time in h	152	143	135	128	122	117	112

be necessary. The burn-in functional stress test screens design and manufacturing weaknesses for the required mission time. Lifetime and burn-in test will be shortened with higher temperature following the Arrhenius relationship.[40] During the test procedure, the satellite software is nominally functional, and the combination of hardware and software can perform its basic mission objectives. This test procedure could be performed either at ambient or at higher temperature. The specific time requirement is shown in Table 6.

For the ambient temperature, the required test time should be greater than 215 h. Because of its rather simple realization, we performed the test at ambient temperature. To be on the safe side, the engineering model was tested up to 430 h with no operation violations and failures of the electronics.

4.3 *Thermal Vacuum Cycling Test*

Thermal vacuum cycling is used to screen problems caused by thermal cycling in orbit. With this method, outgassing problems and thermal dependencies of components can be characterized. The thermal vacuum tests of the qualification model were conducted in accordance with the test conditions and requirements from the satellite provider. Figure 10 shows the interface temperatures and the chamber pressure. Four temperature sensors were attached to the instrument. Temperatures and pressure during all test cycles are given with the corresponding operation times. Hot and cold starts were carried out at +60°C and −40°C, respectively. This is 5 K above maximum and below the minimum operational temperature condition.

With the automotive grade components used in this design, no abnormalities or failures were expected during cycling. However, the cold and warm starts of the electronics might affect specific components such as capacitors with thermal variations, which can cause malfunctions of the voltage converters. The cycling test showed that the ceramic multilayer capacitors with XR7 classification used in design are suitable and worked without any violations. The electronics could reliably be switched on and off and passed all thermal cycles.

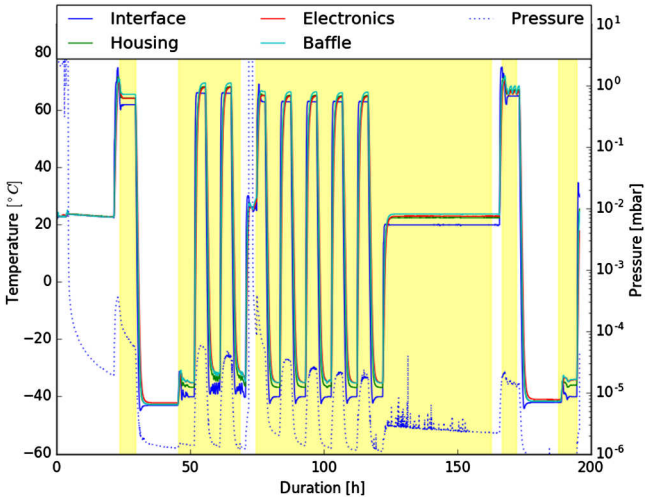

Fig. 10 Thermal-vacuum test temperatures and chamber pressure during all cycles. "On" times are displayed by yellow patches.

Table 7 TID values of sensor electronics with SoM and circuit boards.

device	Dose rate (krad/h)	Accumulated TID (krad)	Fails TID (krad)
SoM – TE0720	1.25 to 2.5	24.95	Pass
FEE PCB – QM	1.25 to 2.5	30.21	Pass
PXE PCB – QM	1.25 to 2.5	30.21	Pass

4.4 *Radiation Test*

A gamma ray test was used for board level screening regarding TID effects of the SoM device to qualify total mission lifetime. Radiation testing for space electronics is typically performed with one of the following radiation types: gamma ray (cobalt-60), proton, and heavy ion. Cobalt-60 generates high-energy gamma rays that contribute to the TID, but do not cause SEE. Proton testing requires a cyclotron capable of accelerating protons and is recommended as a radiation test option, allowing board level testing for TID effects, SEU, and SEFI characterization, and screening for parts with unacceptably low SEL, SEB, or SEGR tolerance.[17] This option comes with higher costs and difficult facility availability. Heavy ion testing fulfils space environment conditions and tends to be expensive and only available in a few locations worldwide. The SEU and SEFI characterization with proton testing was skipped due to an in-orbit verification option.

The cobalt-60 facility at Fraunhofer Institute for Technological Trend Analysis (INT) was used for board level testing. The sensor electronics were classified in modules, which were irradiated in separate irradiation steps with different total dose rates. The board was powered and run in a normal mode during irradiation such that components are biased in a representative condition. If a malfunction inside the electronics occurred, the irradiation steps were interrupted to verify which component or module failed. As a final test, the qualification model was irradiated with dose rates listed in Table 7.

The sensor electronics operated without abnormalities up to a TID of 25 krad. At higher doses, the FPGA configuration crashes due to weakness of the configuration flash memory (Cypress QSPI S25SL256). As a consequence, an additional local aluminum shielding has been installed around the SoM ($d = 1$ mm). The circuit boards FEE and PXE with power distributions, local storage capabilities, and communication interfaces were successfully tested up to 30 krad and the CMOS detector HWK1910 works normally up to 85 krad.

5 Conclusion and Outlook

This paper describes the design procedure for a reliable long-life electronics based on an SoM architecture, which requires less development resources and allows more scientists access to space missions. The sensor electronics can be used for a wide variety of remote sensing instruments in future LEO missions. Integrating most of the functionality to control the science instruments (e.g., hardware logic and software routines) into a single module could improve the reliability and performance with less power consumption. A significant measure is to limit the operation of the system to the required measuring times. Using a detailed radiation environment modeling, a mitigation of failure rates by a factor 4 could be achieved by switching off components during SAA passes, if this is compatible with scientific mission objectives. In addition, essential measures are the triplicated programmable logic and the reconfiguration of the SoM with a reference boot image controlled by a WDT circuit. The system error rate of triplicating logic could be calculated, and our partially mitigated design showed a negligible error rate over mission time. In combination with protection circuits to prevent SEL, a minimalist electronics design is given. In our qualification test, all electronics passed a total dose of 25 krad, which is about twice the expected dose of a 3-year mission. This RDM also accounts for lot-to-lot and part-to-part variation. A more detailed analysis of these variations will enable a better prediction and will be part of our future studies. The presented design is in use in a highly miniaturized limb sounder as a case-study instrument to demonstrate the feasibility of the SoM-based electronics.

A final analysis of the long-term behavior regarding SEU and SEFI interactions is planned after the end of the mission with the AtmoSHINE instrument. With a capability of at least 3 years of mission lifetime, an implementation of the sensor electronics will allow for integrating in further science instruments, such as AtmoCube-A1.[41]

References

1. J. Bouwmeester and J. Guo, "Survey of worldwide pico- and nanosatellite missions, distributions and subsystem technology," *Acta Astron.* **67**(7), 854–862, (2010).
2. A. Poghosyan and A. Golkar, "CubeSat evolution: analyzing CubeSat capabilities for conducting science missions," *Prog. Aerosp. Sci.* **88**, 59–83, (2017).
3. A. Chin et al., "CubeSat: the pico-satellite standard for research and education," in *AIAA SPACE 2008 Conf. & Exposition*, AIAA 2008–7734 (2008).
4. K. Woellert et al., "Cubesats: cost-effective science and technology platforms for emerging and developing nations," *Adv. Space Res.* **47**, 663–684 (2011).
5. B. Fiethe et al., "Reconfigurable system-on-chip data processing units for space imaging instruments," in *Proc. Autom. Test in Europe Conf. 2007 Design Exhibition*, pp. 1–6 (2007).
6. D. Sabena et al., "Reconfigurable high performance architectures: How much are they ready for safety-critical applications?" in *Proc. 19th IEEE Eur. Test Symp. (ETS)*, pp. 1–8 (2014).
7. N. Montealegre et al., "In-flight reconfigurable FPGA-based space systems," in *Proc. NASA/ESA Conf. Adapt. Hardware and Syst. (AHS)*, pp. 1–8 (2015).
8. X. Iturbe et al., "Towards a generic and adaptive system-on-chip controller for space exploration instrumentation," in *NASA/ESA Conf. Adapt. Hardware and Syst.* (2015).
9. F. Taher, A. Zaki, and H. Elsimary, "Design of low power FPGA architecture of image unit for space applications," in *2016 IEEE 59th International Midwest Symposium on Circuits and Systems (MWSCAS)*, pp. 1–4, (2016).
10. M. Deiml et al., "Test of a remote sensing Michelson-interferometer for temperature measurements in the mesosphere on a REXUS rocket," in *23rd ESA Symp. Eur. Rocket and Balloon* (2017).
11. A. Kalman et al., "MISC™– A novel approach to low-cost imaging satellites," in *Proc. AIAA/USU Conf. Small Satellites* (2008).
12. R. Sandau, "Status and trends of small satellite missions for Earth observation," *Acta Astron.* **66**, 1–12 (2010).
13. A. Mahmoud, T. T. Elazhary, and A. Zaki, "Remote sensing CubeSat," *Proc. SPIE* **7826**, 78262I (2010).
14. D. Pack et al., "Two aerospace corporation CubeSat remote sensing imagers: CUMULOS and R3," in *Proc. AIAA/USU Conf. Small Satellites* (2017).
15. P. Preusse et al., "New perspectives on gravity wave remote sensing by spaceborne infrared limb imaging," *Atmos. Meas. Tech.* **2**, 299–311 (2009).
16. C. Venturini, R. D. Santos, and M. Tolmasoff, "Improving mission success of CubeSats," in *U.S. Space Program Mission Assur. Improv. Workshop*, TOR-2017-01689 (2017).
17. D. Sinclair and J. Dyer, "Radiation effects and COTS Parts in SmallSats," in *Proc. AIAA/USU Conf. Small Satellites* (2013).
18. K. A. LaBel et al., "Emerging radiation hardness assurance (RHA) issues: a NASA approach for space flight programs," *IEEE Trans. Nuclear Sci.* **45**(6), 2727–2736 (1998).
19. J. L. Barth, K. A. LaBel, and C. Poivey, "Radiation assurance for the space environment," in *Proc. Int. Conf. Integr. Circuit Design and Technol.*, pp. 323–333 (2004).
20. D. Heynderickx et al., "ESA's Space Environment Information System (SPENVIS): A WWW interface to models of the space environment and its effects," in *Proc. Sun - Earth Connection and Space Weather*, Vol. 75, pp. 245–254 (2000).
21. G. B. Palmerini and F. Pizzirani, "Design of the radiation shielding for a microsatellite," *Acta Astron.* **50**, 159–166 (2002).
22. W. C. Fan et al., "Shielding considerations for satellite microelectronics," *IEEE Trans. Nuclear Sci.* **43**(6), 2790–2796 (1996).

23. K. A. LaBel, J. A. Pellish, and P. J. Majewicz, "NASA electronic parts and packaging (NEPP) program: resources for SmallSats on EEE parts," in *Proc. AIAA/USU Conf. Small Satellites* (2018).
24. J. Guillermin et al., "Part-to-part and lot-to-lot variability study of TID effects in bipolar linear devices," in *16th Eur. Conf. Radiat. and Its Effects on Compon. and Syst. (RADECS)*, pp. 1–8 (2016).
25. M. J. Campola, "Taking Smallsats to the next level - sensible radiation requirements and qualification that won't break the bank," in *Proc. AIAA/USU Conf. Small Satellites* (2018).
26. M. Amrbar et al., "Heavy ion single event effects measurements of Xilinx Zynq-7000 FPGA," in *Proc. IEEE Radiat. Effects Data Workshop (REDW)* (2015).
27. E. L. Petersen et al., "Geometrical factors in SEE rate calculations," *IEEE Trans. Nuclear Sci.* **40**(6), 1888–1909 (1993).
28. A. J. Tylka et al., "CREME96: a revision of the cosmic ray effects on micro-electronics code," *IEEE Trans. Nuclear Sci.* **44**(6), 2150–2160 (1997).
29. G. P. Ginet et al., "AE9, AP9 and SPM: new models for specifying the trapped energetic particle and space plasma environment," in *The Van Allen Probes Mission*, Springer, Boston, Massachusetts, pp. 579–615 (2013).
30. W. R. Johnston et al., "Recent updates to the AE9/AP9/SPM radiation belt and space plasma specification model," *IEEE Trans. Nuclear Sci.* **62**(6), 2760–2766 (2015).
31. K. A. LaBel et al., "Commercial microelectronics technologies for applications in the satellite radiation environment," in *Proc. IEEE Aerosp. Appl. Conf.*, Vol. 1, pp. 375–390 (1996).
32. P. E. Dodd et al., "Current and future challenges in radiation effects on CMOS electronics," *IEEE Trans. Nuclear Sci.* **57**(6), 1747–1763 (2010).
33. J. R. Schwank, M. R. Shaneyfelt, and P. E. Dodd, "Radiation hardness assurance testing of microelectronic devices and integrated circuits: radiation environments, physical mechanisms, and foundations for hardness assurance," *IEEE Trans. Nuclear Sci.* **60**(6), 2074–2100 (2013).
34. L. D. Edmonds, "Analysis of single-event upset rates in triple-modular redundancy devices," Technical report, NASA JPL Publication 09–6 (2009).
35. G. Allen et al., "'Single event test methodologies and system error rate analysis for triple modular redundant field programmable gate arrays," *IEEE Trans. Nuclear Sci.* **58**(3), 1040–1046 (2011).
36. M. Kaufmann et al., "A highly miniaturized satellite payload based on a spatial heterodyne spectrometer for atmospheric temperature measurements in the mesosphere and lower thermosphere," *Atmos. Meas. Tech.* **11**(7), 3861–3870 (2018).
37. D. Nguyen, S. M. Guertin, and J. Patterson, "Radiation tests on 2 Gb NAND flash memories," in *Radiat. Effects Data Workshop*, pp. 121–125 (2006).
38. M. Herrmann, K. Grürmann, and F. Gliem, "Heavy ion SEE test of 4 Gbit DDR3 SDRAM devices," Test report, Technische Universität Braunschweig (2014).
39. R. Kingsbury et al., "TID tolerance of popular CubeSat components," in *Proc. IEEE Radiat. Effects Data Workshop (REDW)*, pp. 1–4 (2013).
40. W. Frazier, R. Rohrschneider, and M. Verzuh, "CubeSat strategies for long-life missions," *in Low-Cost Planet. Missions Conf.* (2013).
41. F. Olschewski et al., "AtmoCube A1: airglow measurements in the mesosphere and lower thermosphere by spatial heterodyne interferometry," *J. Appl. Remote Sens.* **13**(2), 024501 (2019)

Biographies of the authors are not available.